ELSEVIER

Ultramicroscopy 72 (1998) 223–232

ultramicroscopy

The contrast of images formed by atomic focusers

J.M. Cowley*, R.E. Dunin-Borkowski[1], Michele Hayward[2]

Department of Physics and Astronomy, Arizona State University, Box 871504, Tempe, AZ 85187-1504, USA

Received 17 November 1997; received in revised form 10 February 1998

Abstract

The feasibility of the various modes for using atomic focusers to attain resolutions of 0.5 Å or better in TEM or STEM instruments, as proposed in a previous paper [Cowley, Spence and Smirnov, Ultramicroscopy 68 (1997) 135], has been confirmed in two ways. Firstly, theoretical expressions for the image contrast have been derived using a simple, justifiable, approximation for the transmission function of the focusers and show that components of the image intensity functions with the desired resolution exist. Secondly, computer simulations of the imaging for specimens consisting of pairs of gold atoms have demonstrated resolutions of 0.5 Å or better, with good contrast, for the modes involving the placing of the specimen at a Fourier image distance from a crystal multiple atomic focuser.

1. Introduction

In a previous paper [1], it was suggested that the initial idea of using single atoms, or lines of atoms passing through a thin single crystal, as "atomic focusers" to form ultra-high-resolution images [2] could be exploited in a number of ways which might allow the attainment of resolutions of the order of 0.05 nm by relatively small modifications of existing transmission or scanning transmission (TEM or STEM) instruments. Although the previous paper [1] contained several computer-based simulations suggesting confirmation of the essential assumptions of the various imaging schemes, it did not provide detailed treatments of the image formation in the various instrumental modes. Nor did it provide any simulations of the images that would be formed for particular cases. In the present paper, we offer some further theoretical treatments of the imaging process based on reasonable assumptions for several of the proposed imaging modes and some computer simulations suggesting the contrast and resolutions that should be attainable for particular test objects.

We consider, in turn, the various schemes for TEM and STEM imaging, making use of the atomic focuser principles, as described in the previous paper. We start with the use of a single atomic

* Corresponding author: Tel.: + 1 602 965 6459; fax: + 1 602 965 7954; e-mail: cowleyj@asu.edu.

[1] Also at: Center for Solid State Science, Arizona State University, USA.

[2] Present address: Department of Physics, Taylor Hall, The College of Wooster, Wooster, OH 44691, USA.

0304-3991/98/$19.00
PII S0304-3991(98)00019-9

focuser in combination of a piezo-electric specimen manipulation system such as is used in STM and related scanning-probe microscopies, and then continue with the various schemes involving a crystal multiple-focuser arrangement and the associated Fourier-image phenomenon which may simplify the problem of obtaining relative motions of the focuser and the specimen. In this paper we do not discuss the instrumental factors and experimental arrangements required for successful realization of the various schemes, but offer some results which may help define the requirements for their future practical exploitation.

From the reciprocity relationship, it is to be expected that, if a very fine probe is formed by an atomic focuser and can serve to form a ultra-high-resolution STEM image of a specimen, then the atomic focuser can act as a TEM imaging device, at least for the paraxial situation (see Fig. 4 of Ref. [1]). It does not necessarily follow that the TEM image formed in this way will have a field of view sufficiently large to make use of atomic-focusers in TEM systems a feasible option. This topic has been addressed in another paper which reports computer simulations aimed at determining the limitations of the contrast, resolution and field of view of atomic-focuser TEM systems as a function of the specimen position and the thickness of a crystal used to form the atomic-focuser elements [3].

In general, it may be noted that the dimensions of the probes, or the resolutions of the images, formed by atomic focusers are approximately the same as the dimensions of the peaks of projected potential of the atoms to be imaged (see Fig. 1 of Ref. [1]). In reciprocal space, it may be considered that the radius of the effective aperture of the atomic focuser, considered as a lens, is about 2–3 $Å^{-1}$. As indicated in Fig. 1, the atomic scattering factors have fallen off to about 0.1 of their maximum values in this range. It may be considered that, because of the two-dimensional nature of the scattering distribution, the total contribution of an atom to an image may more rightly be considered to be proportional to $2\pi uf(u)$, where $|u| = (2\sin\theta)/\lambda$, and θ is half the scattering angle. As seen in Fig. 1, the multiplication by u, especially for heavy elements such as Au, gives much greater emphasis to the high-angle scattering, but this must

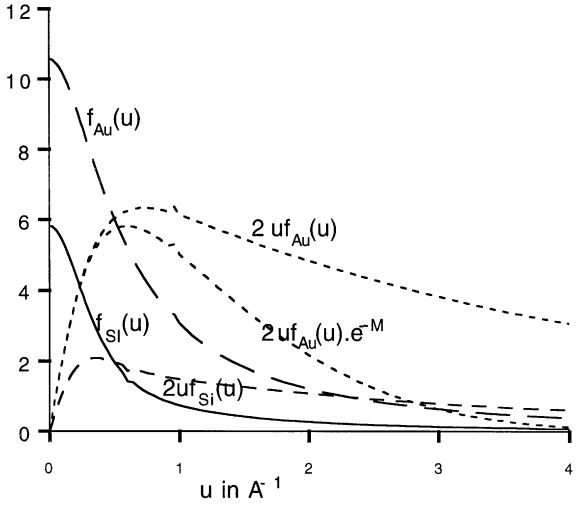

Fig. 1. Atomic scattering factors, $f(u)$, and the functions $uf(u)$ for Au and Si atoms, modified by the Debye–Waller factor in the case of Au.

be modified by the Debye–Waller factor. Also, for a line of atoms through a crystal, the angular extent of the scattering may be increased or decreased by a factor of about 2 by dynamical scattering effects. Hence, it may be concluded that the atomic focuser images should include most of the information available from the elastic scattering of electrons by atoms.

2. STEM with a single atomic focuser

The original concept for the use of atomic focusers [2] envisaged the use of a single heavy atom, or a row of atoms passing through a thin crystal to concentrate the focussed beam from a STEM instrument to form a probe of very small diameter which could be used to give very high-resolution STEM imaging. It was reported in Ref. [1] (see Fig. 1 of Ref. [1]), that one-dimensional calculations suggest that, for a crystal of suitable thickness, probe sizes of diameter less than 0.5 Å may be formed in this way when one plane of the atoms in a crystal is illuminated by a STEM beam of diameter about 2 Å. Since then, two-dimensional calculations for a STEM beam incident on a gold crystal in various orientations [3] and for a barium

crystal in [0 0 1] orientation (for which the distance between atom positions in projection is 3.5 Å) have shown that, as found by other authors for various crystals [4,5], the wave leaving the crystal exit face for suitable thicknesses is sharply peaked with a diameter of less than 0.5 Å and a very low background.

A further feature of the exit wave is that, as for the probe in a normal STEM instrument, the phase of the exit wave is very nearly constant across the amplitude peak. This constant value of the phase increases to π, relative to a constant background value, as the crystal thickness increases to the optimum value giving the sharpest intensity peak. The amplitude and phase of the wave formed at the exit face of an Au [0 0 1] crystal, 28 Å thick, for a plane wave incident are shown in Fig. 2. It is therefore a good approximation to model the transmission function of the atomic focuser as a real function, $p(x, y)$ added to a constant, complex background, $H = J + iK$, as suggested in Fig. 3, for simulations of the intensity in the STEM detector plane. (A similar factorization of the exit wave function into the incident probe and some channelling function has been described and discussed by Broeckx et al. [6]). For illumination by a STEM instrument having an objective-lens transfer function $T(u)$ (considered in one dimension for convenience), and a spread function $t(x) = c(x) + is(x)$, where $c(x)$ and

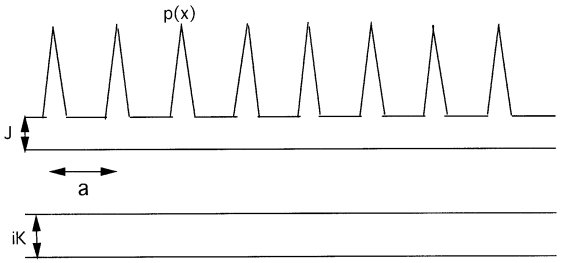

Fig. 3. Real and imaginary parts of a model transmission functions for a crystal multiple focuser, with peaks $p(x)$ added to a constant complex background, $H = J + iK$.

$s(x)$ are real functions, the wave incident on the specimen is then $t(x)\{H + p(x)\}$. For a thin specimen, the transmission function may be taken as $q(x) = \exp\{-i\sigma\varphi(x)\}$ with Fourier transform $Q(u)$. The intensity distribution on the plane of observation, when the focuser is translated by an amount X relative to the specimen, is given by

$$\begin{aligned} I_X(u) &= |\mathrm{Ft}[t(x)\{H + p(x - X)\}q(x)]|^2 \\ &= |H|^2|T(u) * Q(u)|^2 + |T(u) * Q(u) * P(u) \\ &\quad \times \exp\{2\pi i u X\}|^2 + 2\mathrm{Re}[H^*\{T^*(u) * Q^*(u)\} \\ &\quad \times \{T(u) * Q(u) * P(u) \exp(2\pi i u X)\}], \end{aligned} \tag{1}$$

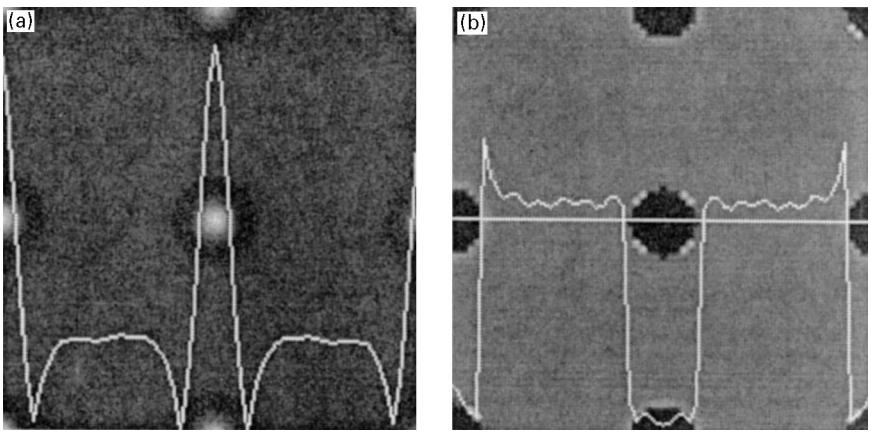

Fig. 2. Calculated amplitude (a) and phase (b) distributions at the exit face of a 28 Å thick Au [0 0 1] crystal for an incident plane wave. The profile across the central Au atom is superimposed on the two-dimensional image. For the phase, the vertical limits of the diagram represent $-\pi$ and $+\pi$.

where Ft indicates a Fourier transform, $P(u)$ is the Fourier transform of $p(x)$, Re is the real part of the function, and the $*$ sign, on line, indicates a convolution integral. The STEM signal produced by the focuser is then given by integrating the intensity over the aperture, $D(u)$, of the detector for each position, X, of the focuser relative to the specimen:

$$J(X) = \int I_X(u)D(u)\,\mathrm{d}u. \tag{2}$$

As in normal STEM theory [7] the bright-field image may be approximated by assuming the detector function to be a delta function, on axis, $D(u) = \delta(u)$. Applying this to the first term of Eq. (1) gives just a constant term, equal to the total intensity of the incident beam for a weak-phase object, $q(x) = 1 - \mathrm{i}\sigma\varphi(x)$. The contribution of the second term of Eq. (1) to the BF STEM image is

$$\{p(X) * (q(X)t(X))\} * \{p(X) * (q^*(X)t^*(X))\} \tag{3}$$

and for a weak-phase object this gives an image of the projected potential distribution convoluted by $\{t(X) * p(X)\}$ which, because $p(X)$ is much narrower than $t(X)$, is very close to being just $t(X)$ so that this term is close to being a normal STEM image of $\sigma\varphi(X)$.

The ultra-high-resolution components of the image appear in the third, cross-product term of Eq. (1). For a weak-phase object, putting $S = \int s(X)\sigma\varphi(X)\,\mathrm{d}X$ and $C = \int c(X)\sigma\varphi(X)\,\mathrm{d}X$, this becomes

$$\begin{aligned} &2J[\{1+S\}\,\{p(X) * c(X) + p(X) * (\sigma\varphi(X)\,s\,(X))\} \\ &- C\{p(X) * s(X) + p(X) * (\sigma\varphi(X)\,c\,(X))\}] \\ &- 2K[(1+S)\,\{p(X) * s(X) + p(X) * (\sigma\varphi(X)\,c\,(X))\} \\ &+ C\{p(X) * c(X) + p(X) * (\sigma\varphi(X)\,s\,(X))\}]. \end{aligned} \tag{4}$$

For a phase difference of π between the peak $p(X)$ and the background, as in the optimum case of imaging illustrated in Fig. 2, $K = 0$, and for the optimum defocus of the illuminating STEM beam, for which $s(X)$ is a large negative peak and $c(X)$ is small, the first-order component of Eq. (4) reduces to

$$2Jp(X) * (\sigma\varphi(X)\,s\,(X)), \tag{5}$$

which represents an image of the illuminated region of the sample with a resolution limited by the width of the $p(X)$ peak. For the "mimium contrast", in-focus setting of the STEM for which it can be assumed that $s(X) = 0$, the corresponding contribution to the image is $2J\{p(X) * c(X)\}$, which is a low-resolution form of a normal STEM image of the $p(X)$ function, independent of the specimen.

For a different thickness of the atomic focuser, it may be that the phase difference of $p(X)$ relative to the background is an odd multiple of $\pi/2$, so that $J = 0$. Then there is an ultra-high-resolution component of the image for both the minimum-contrast position and the optimum defocus position, for which the components are, respectively,

$$2K[p(X)*\sigma\varphi(X) + C\{p(X)*c(X)\}]$$

and

$$2K[(1+S)\{p(X) * s(X)\} + \{p(X) * (\sigma\varphi(X)\,s\,(X))\}]. \tag{6}$$

This suggests that a first-order ultra-high-resolution imaging of the projected potential will be given for most values of the phase factor H and for most defocus values of the illuminating STEM probe. The contrast of the ultra-high-resolution images for particular cases may be determined from computer simulations. The reciprocity relationship, however, suggests that the contrast observed is the same as for the TEM single-focuser case which has been simulated, as reported in [3] and has shown useful contrast for single-atom specimens.

The assumption of a very small detector, approximated by a delta function, implies that the signal strength for the BF STEM imaging is very small. In practice, for normal STEM, it is convenient to use a detector aperture which accepts an appreciable fraction of the incident beam spot of the diffraction pattern so that the image signal strength is convenient. As has been shown earlier, [6], the effect of increasing the detector aperture diameter is to decrease the contrast of the BF image, slowly at first and then rapidly, to give zero contrast for weak-phase objects when the detector accepts all the central beam. The resolution improves slightly with increasing detector size. A suitable compromise is then usually found to give the

most desirable balance of image intensity, resolution and contrast for any particular application. It is anticipated that the same considerations will apply for the ultra-high-resolution STEM imaging with atomic focusers.

For dark-field imaging, the situation is different from that of normal STEM in which the central beam spot of the diffraction pattern is an image of the STEM objective aperture. For an atomic focuser, illuminated by a STEM beam, there is a similar central spot given by the back-ground term, H, but the more important component part of the "central spot", related to the ultra-high-resolution imaging, is given by $|P(u)|^2$, which is a continuous, broad distribution of half-width about 2 or 3 $Å^{-1}$. The convolution with $Q(u)$ in Eq. (1) then gives a similar, but somewhat broader distribution. For a weakly scattering object, the use of any annular detector will therefore give a large background plus a small positive or negative signal due to the object, depending on the relative phase and on whether the detector includes the inner part or outer part of the intensity distribution.

A more effective form of detector may be a split detector, omitting the central part of the diffraction pattern which is the image of the objective aperture due to H, and divided along a line perpendicular to the direction of the beam scan giving a signal produced by subtraction of the signal from one half-detector from the signal from the other half, as in the case of the "differential contrast" detectors developed, for example, by Chapman et al. [8].

Thus, for a weak-phase object, assuming that $P(u)$ is real and that $Q(u)\,(=\delta(u)+\mathrm{i}\sigma\Phi(u))$ is symmetrical, as for a single atom, the intensity distribution in the plane of observation due to the focuser peak is

$$I(u) = P^2(u) + |P(u)\exp\{2\pi\mathrm{i}uX\} * Q(u)|^2 + 2\sigma P(u)[P(u) * (\Phi(u)\sin 2\pi uX)\}. \quad (7)$$

In this, the first two terms are even in u and the third is odd. Hence, with a split detector, and with the signals for positive and negative u being subtracted, the first two terms give no contribution to the signal as a function of X and the last term gives a signal proportional to the first power of $\Phi(u)$ which is antisymmetric about the atom position and has a width depending on that of $p(X)$ in both the beam-scan direction and at right angles. The main limitation to such a first-order imaging system may well be the noise from the subtraction of the two large background signals.

3. TEM with fourier images of crystal multiple focusers

As a means for avoiding the difficulties associated with translating a specimen held at a distance of about 20 Å from an atomic focuser, it was envisaged [1] that, if a thin crystal multiple focuser is used, the specimen may be placed at the position of one of the Fourier images formed by the periodic exit wave from the crystal. Then the distance of the specimen from the crystal focuser may be of the order of 1000 Å, and the periodic array of fine probes can be translated across the specimen by tilting the plane-wave beam incident on the crystal. The necessary mechanical stability of the specimen relative to the crystal focuser may then be assured by attaching the specimen firmly to the crystal. The ultra-high-resolution image data is then collected by using a normal high-resolution TEM to record a set of images with different tilts of the incident beam (see Fig. 5 of Ref. [1] and Fig. 4).

Analytical expressions for the intensities of the TEM images formed with this system may be made using reasonable approximations for the wave produced by the crystal focuser, as in Fig. 3. Since, as in Fig. 2, it has been shown that the phase is constant across the sharp central peak of intensity formed at the atomic positions for a crystal of optimum thickness, the exit wave from the crystal can be modelled as

$$\psi_e(x) = \exp\{2\pi\mathrm{i}u_0x\}\left[H + \sum_n p(x) * \delta(x - na)\right], \quad (8)$$

where u_0 indicates the incident beam tilt, $p(x)$ is the real amplitude peak function, a is the crystal periodicity and H is a constant background, assumed to be complex, $H = J + \mathrm{i}K$, in order to allow for the phase difference of the peak relative to the background. For a distance R between the crystal and the specimen which has a transmission

function $q(x)$, the wave function in the image plane of the TEM instrument, which has a transfer function $T(u)$ and a spread function $t(x)$, is then given by

$$\psi(x) = q(x)\left[\exp\{2\pi i u_0 x\}\left\{H + \sum_n p\,(x - na)\right\} * \exp\{-\pi i x^2/R\lambda\}\right] * t(x). \quad (9)$$

If R is a Fourier image distance, substituting $R = 2na^2/\lambda$, in this expression gives, with a little manipulation, the TEM image intensity as

$$I(x) = \left|Hq(x)\exp\{2\pi i u_0 x\} * t(x) + \left\{\sum_n p\,(x + R\lambda u_0 - na)\,q\,(x) \times \exp\{2\pi i u_0 x\} * t(x)\right\}\right|^2. \quad (10)$$

The square of the first term in this expression, for u_0 small, is just the normal bright-field image of the specimen, giving the intensity distribution $|H|^2|q(x) * t(x)|^2$. If the specimen is a weak-phase object, $q(x) = 1 - i\sigma\phi(x)$ and $t(x)$ is written as $t(x) = c(x) + is(x)$, where c and s are real, this takes the familiar form

$$I_1(x) = |H|^2[1 + 2\sigma\varphi(x) * s(x)]. \quad (11)$$

The square of the last term of Eq. (10), for a weak-phase object, becomes

$$I_2(x) = \left(\sum_n p\,(x + R\lambda u_{0-} - na) * c(x)\right)^2 + \left(\sum_n p\,(x + R\lambda u_0 - na) * s(x)\right)^2 - \left\{\sum_n p\,(x + R\lambda u_0 - na) * c(x)\right\} \times \left\{\sigma\varphi(x)\sum_n p\,(x + R\lambda u_0 - na) * s(x)\right\} + \left\{\sum_n p\,(x + R\lambda u_0 - na) * s(x)\right\} \times \left\{\sigma\varphi(x)\sum_n p\,(x + R\lambda u_0 - na) * c(x)\right\}. \quad (12)$$

In this expression, the first two terms give a normal TEM image of the crystal focuser, as if no specimen were present. The last two terms give first-order images of the projected potential of the specimen, sampled by the set of ultra-fine probes. It may be noted that the expression containing $s(x)$ is multiplied by one containing $c(x)$ and vice versa. Since $s(x)$ is very small when $c(x)$ is a maximum and $c(x)$ is small when $s(x)$ is a maximum (optimum defocus), and these two terms are of opposite sign, the total contribution of these terms may be small.

Writing, for brevity, $f(x) = \sum_n p\,(x + R\lambda u_0 - na)$, the cross-product term of Eq. (10) becomes, for small u_0,

$$I_3(x) = 2\mathrm{Re}\,[(J - iK)\{q^*(x) * t^*(x)\} \times \{(f(x)\,q(x)) * t(x)\}] \quad (13)$$

and for the weak-phase-object approximation, this gives

$$+ 2[\{f(x) * c(x)\}\{J(1 - \sigma\varphi(x) * s(x)) - K(\sigma\varphi(x) * c(x))\} + \{f(x) * s(x)\}\{J(\sigma\varphi(x) * c(x)) + K(1 - \sigma\varphi(x) * s(x))\} + \{(\sigma\varphi(x)f(x)) * s(x)\} \times \{J(1 - \sigma\varphi(x) * s(x)) - K(\sigma\varphi(x) * c(x))\} - \{(\sigma\varphi(x)f(x)) * c(x)\}\{J(\sigma\varphi(x) * c(x)) + (1 - \sigma\varphi(x) * s(x))\}]. \quad (14)$$

In this expression, the desired terms, giving rise to the ultra-high-resolution image, are those in $\sigma\varphi(x)\,f(x)$, involving the sampling of the projected potential by the periodic array of very fine probes. These terms are weighted according to the phase of the fine probes and the focus of the microscope that views them. It has been seen that, as in Fig. 2, the phase of the probes, relative to the background may be π for an optimum crystal thickness, in which case $J = -1$ and $K = 0$, so that this term (14), becomes

$$- 2\{f(x) * c(x)\}\{1 - \sigma\varphi(x) * s(x)\} - 2\{f(x) * s(x)\}\{\sigma\varphi(x) * c(x)\}. - 2\{(\sigma\varphi(x)f(x)) * s(x)\}\{1 - \sigma\varphi(x) * s(x)\} + 2\{(\sigma\varphi(x)f(x)) * c(x)\}\{\sigma\varphi(x) * c(x)\}. \quad (15)$$

For the Scherzer optimum defocus of the microscope, $s(x)$ is a large negative peak but $c(x)$ is small and broad and, to a first approximation, can be neglected. This term then becomes

$$-2(\sigma\varphi(x)f(x)) * s(x), \tag{16}$$

so that there are resolved peaks in the microscope image of intensity depending on the sampling of the projected potential by the set of ultra-fine probes. Putting $f(x) = f(x+\eta)$, where $\eta = R\lambda u_0$, and integrating each of the peaks, $s(x)$, of the TEM image to give s_0, the variation of the signal as a function of the angle of incidence is seen to give $-2s_0\sigma\varphi(\eta) * p(\eta)$.

For the defocus ("in focus") corresponding to minimum contrast in normal TEM WPOA images, it is a good approximation to put $s(x) = 0$, and the only terms remaining in Eq. (15) are of second order in $\sigma\varphi$ and are therefore negligibly small.

For a different crystal thickness, the phase difference of the probes relative to the background may be an odd multiple of $\pi/2$, in which case $J = 0$ and $K = 1$ (or -1). With these values inserted in Eq. (14), it is seen that for the "optimum defocus" the intensity term is

$$-2\{f(x) * s(x)\}\{1 - \sigma\varphi(x) * s(x)\} \tag{17}$$

and this represents a low contrast normal TEM image of the specimen, modulated by a TEM image of the set of probes. The "in focus" image, however, contains, in addition, the term

$$-2\sigma(\varphi(x)f(x)) * c(x), \tag{18}$$

which is almost as favorable as Eq. (16) if the TEM used is able to resolve the periodicity of $f(x)$ in the in-focus condition. Again, the variation of the integrated value for each TEM peak with the angle of incidence gives a signal proportional to $\varphi(\eta) * p(\eta)$.

Thus, the terms (16) or (18) allow a sampling of the object transmission function with the super-high-resolution at sets of periodically-spaced positions, and the translation of these sets of positions by tilting the incident beam allows the complete ultra-high-resolution image of the object to be derived (Fig. 4). These terms are superimposed on constant background terms and terms representing the images with normal TEM resolution of the specimen. The relative magnitudes of the background, the ultra-high-resolution parts and the normal TEM resolution parts of the image are best found by computer simulations for representative cases.

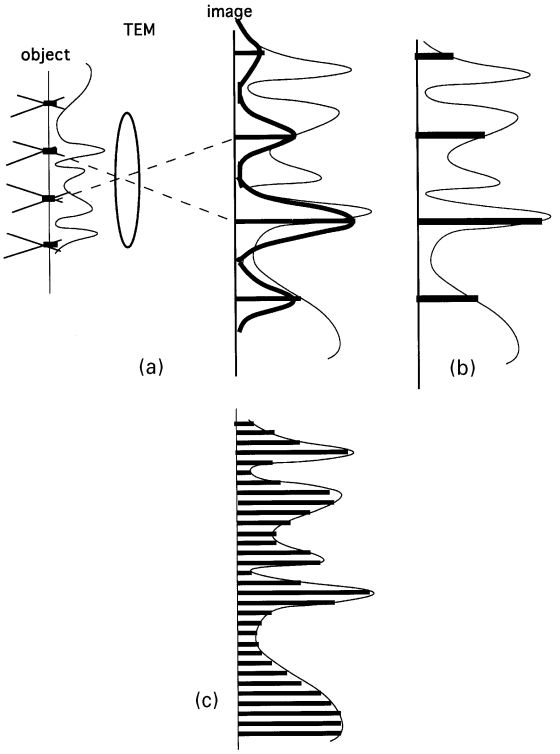

Fig. 4. (a) Diagram illustrating the crystal-focuser TEM scheme. The specimen is illuminated by the array of very fine cross overs and for each cross over the TEM gives an image of normal TEM resolution on the image plane. For each peak a corresponding intensity value is assigned to the peak-center position as in (b). The sets of values found for all incident-beam tilts are correlated to form the ultra-high-resolution image (c).

This imaging process has been simulated for an idealized case. The amplitude distribution in a set of very fine probes formed at a Fourier image distance of 332 Å from an Au [0 0 1] crystal is simulated for various angles of incidence of a plane wave. This set of fine probes passes through the specimen, consisting of two gold atoms separated by 0.5 Å in the y-direction, repeated with the periodicity of 4.07 Å of the Au unit cell. The heights of the corresponding peaks in the image of the

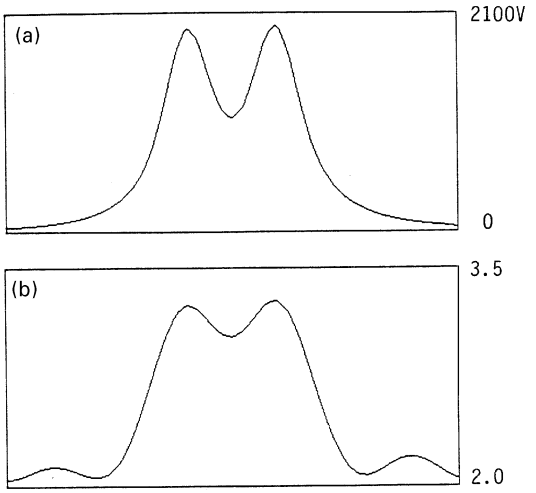

Fig. 5. Simulated image for the crystal-focuser TEM scheme (Fig. 4). Two Au atoms 0.5 Å apart, are placed at the Fourier image distance of 332 Å after an Au [0 0 1] crystal and the TEM peak intensity is plotted as a function of incident beam tilt. (a) The projected potential distribution. (b) The simulated image profile. Total image width is 2.54 Å.

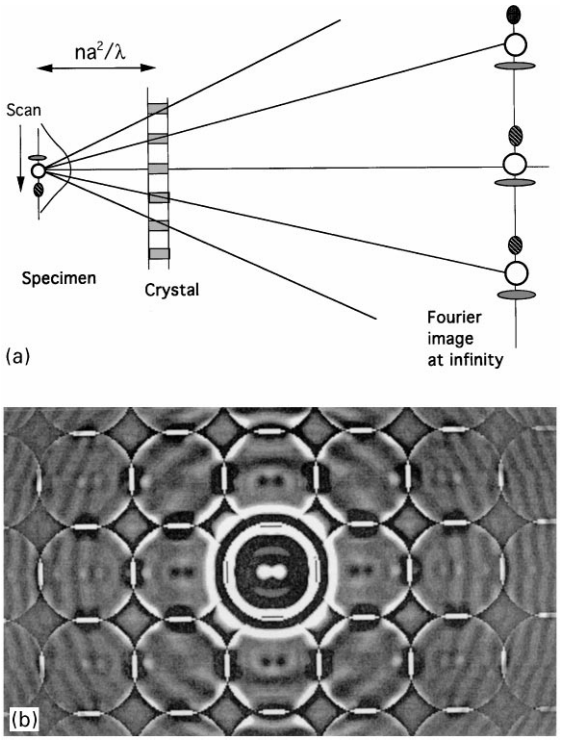

Fig. 6. (a) Simplified diagram for the STEM crystal-focuser case. (b) Image formed for a specimen consisting of two Au atoms, 0.68 Å apart, illuminated by a STEM beam (200 keV, $C_s = 1$ mm) and placed at the Fourier image distance of 332 Å from an Au [0 0 1] crystal, 2.8 nm thick.

sampled specimen, formed with a TEM having $C_s = 1$ mm, with 200 kV electrons, an underfocus of 410 Å (which appeared to give the best images) and an objective aperture semi-angle of 40 mrad, are then found as a function of the angle of tilt of the incident beam. The plot in Fig. 5b, representing the reconstruction from a series of TEM images, suggests that the two Au atoms, 0.5 Å apart, should be clearly resolved.

4. Fourier images at infinity for STEM and a crystal multiple focuser

A further scheme described in Ref. [1], for using a crystal multiple atomic focuser to obtain ultra-high-resolution imaging may be considered as related to that described in Section 3, above, by the reciprocity relationship. A focused beam from a standard STEM instrument, having a resolution for normal STEM imaging of the order of 2 Å, illuminates a specimen which is held at a Fourier image distance from a thin-crystal multiple focuser. A Fourier image of the focuser crystal is formed at infinity beyond the crystal and an image of the specimen is formed in this Fourier image plane with a resolution given by the probe-size formed by an atomic-focuser element (Fig. 6). As shown in Fig. 7 of Ref. [1], the variation of intensity with the direction of the detector element in this case is related by reciprocity to the variation of image intensity with angle of incidence of the beam in the previous scheme.

The essential components of this scheme are represented in Fig. 6a. The beam from the STEM instrument gives an incident wave function, $t(x)$, the Fourier transform of the objective lens transfer function, $T(u)$, so that the wave leaving the specimen is $\psi_0(x) = t(x)\, q(x)$. This wave is propagated over a distance R to the crystal focuser which has a transmission function, modelled, as in Fig. 3b by a constant background term, $H = J + iK$, plus an

array of sharp peaks, $f(x) = \sum_n p(x - na)$. The wave leaving the crystal focuser is

$$\psi(x) = [\psi_0(x) * \exp\{-\pi i x^2/R\lambda\}]\,[H + f(x)\}. \quad (19)$$

The intensity distribution at infinity is then given by the square of the Fourier transform of Eq. (19) as

$$|\Psi|^2 = |H\Psi_0^2| + |\Psi_0(u) \exp\{\pi i R\lambda u^2\} * F(u)|^2 + 2\mathrm{Re}\,[H^*\Psi_0^* \exp\{-\pi i R\lambda u^2\}\,\{\Psi_0(u) \times \exp\{\pi i R\lambda u^2\} * F(u)\}]. \quad (20)$$

The first term of this expression represents the convergent beam diffraction pattern of the object in the absence of a focuser crystal. For the case that the object is at a Fourier image distance from the crystal, so that $R = 2na^2/\lambda$, the second term reduces to

$$|\Psi_0(u) * F(u)|^2 = |\mathrm{Ft}\,\{t(x)\,q(x)\,f(x)\}|^2, \quad (21)$$

where Ft indicates a Fourier transform. This term represents a broad background consisting of a convergent beam diffraction pattern of the focuser crystal plus, for a weak-phase object, a small component depending on $\sigma\varphi(x)$ which is smeared out because the detailed structure of the specimen, is supposed to be on a smaller scale than $t(x)$ or the periodicity of $f(x)$.

The third, cross-product, term of Eq. (20) reduces, with $y = R\lambda u$, to

$$2\mathrm{Re}[\{H^*T^*(y/R\lambda) * Q^*(y/R\lambda)\}\,\{(q(y)\,t(y)) * f(y)\}]. \quad (22)$$

For a sufficiently small range of y, it may be assumed that $T^*(y/R\lambda)$ is unity. For example, for the Fourier image distance for Au [0 0 1] of 332 Å and 200 keV electrons, $R\lambda = 8$ Å^2, and if it is asumed that $T(u)$ is unity out to $u = 0.3$ Å^{-1}, $T^*(y/R\lambda)$ is unity out to a radius of $y = 2.7$ Å. For a weak-phase object, the convolution with $\sigma\Phi(u)$ gives $\sigma\varphi(0)$, and Eq. (22) reduces to

$$2f(y) * [J\{c(y) + \sigma\varphi(y)\,s(y) - \sigma\varphi(0)\,(s(y) - \sigma\varphi(y)\,c(y))\} + K\{s(y) - \sigma\varphi(y)\,c(y) + \sigma\varphi(0)(c(y) + \sigma\varphi(y)\,s(y))\}]. \quad (23)$$

Then, for the phase difference π of the peaks of $f(x)$ relative to the background, and for the optimum focus position for which we may neglect $c(y)$, this term gives

$$-2\sigma f(y) * \{s(y)\,[\varphi(0) + \varphi(y)]\}, \quad (24)$$

which gives an image of the projected potential with white spots for atoms and a resolution governed by the width of the peaks of $f(y)$. For the minimum-contrast defocus, putting $s(y) = 0$, there is no contrast due to the projected potential.

For the phase difference of the peaks of $f(y)$ relative to the background equal to an odd multiple of π/2, i.e., $J = 0$, there is no imaging of the projected potential for the "optimum defocus" position, but for the "minimum-contrast" defocus, the contrast is given by

$$-2\sigma f(y) * [c(y)\{\varphi(0) + \varphi(y)\}], \quad (25)$$

which, again, gives an ultra-high-resolution image of the object.

A simulation of a particular case for this imaging mode has been made for a sample consisting of two gold atoms, separated by a distance of 0.68 Å and illuminated by a STEM instrument with $C_s = 1$ mm for 200 keV electrons with optimum defocus. This specimen is placed at the Fourier image distance of 332 Å from an Au [0 0 1] crystal multiple atomic focuser. The exit wave from the focuser is calculated and then Fourier transformed to give the intensity distribution in the Fourier image formed at infinity which should contain the image of the specimen.

The result of this calculation is given in Fig. 6b for an objective aperture radius of 6.5 mrad. The image of the two gold atoms is seen with good contrast at the center of the image in a region of uniform background of diameter approximately 2 Å. Outside of this region the intensity distribution is complicated in a way that can be understood from the consideration of the other factors in the above equations. The modulation of the intensity by the $T^*(y/R\lambda)$ term in Eq. (22) gives a reversal of phase with increasing $|y|$ which is evident because the image of the two atoms appears with a contrast which reverses with increasing radius. The intensity term, Eq. (21), was said to be a CBED pattern of the crystal multiple focuser and this can be seen as the

set of slightly overlapping disks in the background of Fig. 6b. If a larger objective aperture size is used in the simulation the overlapping of the disks is greater. The areas of overlap are more prominent and tend to dominate the intensity distribution and also decrease the area of nearly constant intensity around the central image of the two atoms.

5. Discussion and conclusions

Analytical expressions have been derived for image intensity distributions for various atomic-focuser systems using a simple model (Fig. 3), which, as suggested by Fig. 2, can give a good representation for the transmisssion function of an atomic focuser. The expressions obtained suggest that the intensities and contrast for the ultra-high-resolution images of weak-phase objects may be comparable with that of normal-resolution images for analogous objects. The contrast depends on the magnitude of the background terms, as in normal TEM or STEM BF imaging and depends on the focal settings of the TEM or STEM instruments used in conjunction with the atomic focusers. The form of the images produced may then best be found for simulations of the imaging processes for particular cases.

For the simulated images, we have assumed the specimens to be composed of gold atoms and, although individual gold atoms are not considered to be described well by the weak-phase-object approximation, they are familiar objects which may serve the purpose of relating the expectations of contrast to those for familiar imaging situations. Simulations confirm the production of images of single gold atoms with good contrast and, for assemblies of gold atoms, the resolution is seen to be better than 0.5 Å, as predicted.

Resolutions of this order can be obtained for 100–400 keV electrons only with beam convergences, or effective objective aperture sizes, of the order of 10^{-1} rad. The depth of focus of the imaging systems must therefore be limited to about 1 nm. This has been confirmed in the simulations made for various schemes. It may present problems in terms of specimen preparation and the manipulation of specimen positions relative to the focuser, but may also offer significant advantages for the three-dimensional imaging of suitable light-atom objects or for the imaging of surface layers of thin films.

Special situations may well arise for the imaging of periodic objects in that there may be Fourier-image formation for both the object and the crystal multiple focuser. Moire patterns can be formed for unequal periodicities of the object and focuser and these may produce ultra-high resolution detail in enlarged images under suitable circumstances [9].

The analyses and simulations presented here suggest that comparable resolutions and contrast may be achieved in any one of a number of experimental modes. The choice of mode, in practice, will be governed mostly by the experimental factors concerned with the preparation and manipulation of suitable specimens and positioning of the specimens in relation to the atomic-focuser crystals. Various means for overcoming these experimental problems are currently under consideration.

Acknowledgements

Participation in this project by M.H. was made possible by the Research Experience for Undergraduates Program of the Department of Physics and Astronomy, ASU, supported by the National Science Foundation and ASU. We thank Paul Perkes for assistance with the computing and the Center for High Resolution Electron Microscopy, ASU, for use of its facilities.

References

[1] J.M. Cowley, J.C.H. Spence, V.V. Smirnov, Ultramicroscopy 68 (1997) 135.
[2] V.V. Smirnov, submitted.
[3] M. Sanchez, J. M. Cowley, Ultramicroscopy 72 (1998) 213.
[4] J. Fertig, H. Rose, Optik 59 (1981) 407.
[5] R.F. Loane, E.J. Kirkland, J. Silcox, Acta Crystallogr. A 44 (1988) 912.
[6] J. Broeckx, M. Op de Beeck, D. Van Dyck, Ultramicroscopy 60 (1995) 71.
[7] J.M. Cowley, A.Y. Au, in: O. Johari (Ed.), Scanning Electron Microscopy, vol. 1, SEM Inc., AMF O'Hare, Illinois, 1978, p. 53.
[8] J.N. Chapman, R. Ploessl, D.M. Donnet, Ultramicroscopy 47 (1992) 331.
[9] J.M. Cowley, A.F. Moodie, Acta Crystallogr. 12 (1959) 423.